GEOLOGY

Experimental evidence supports mantle partial melting in the asthenosphere

10.1126/sciadv.1600246

Julien Chantel,[1]*† Geeth Manthilake,[1] Denis Andrault,[1] Davide Novella,[1]‡ Tony Yu,[2] Yanbin Wang[2]

The low-velocity zone (LVZ) is a persistent seismic feature in a broad range of geological contexts. It coincides in depth with the asthenosphere, a mantle region of lowered viscosity that may be essential to enabling plate motions. The LVZ has been proposed to originate from either partial melting or a change in the rheological properties of solid mantle minerals. The two scenarios imply drastically distinct physical and geochemical states, leading to fundamentally different conclusions on the dynamics of plate tectonics. We report in situ ultrasonic velocity measurements on a series of partially molten samples, composed of mixtures of olivine plus 0.1 to 4.0 volume % of basalt, under conditions relevant to the LVZ. Our measurements provide direct compressional (V_P) and shear (V_S) wave velocities and constrain attenuation as a function of melt fraction. Mantle partial melting appears to be a viable origin for the LVZ, for melt fractions as low as ~0.2%. In contrast, the presence of volatile elements appears necessary to explaining the extremely high V_P/V_S values observed in some local areas. The presence of melt in LVZ could play a major role in the dynamics of plate tectonics, favoring the decoupling of the plate relative to the asthenosphere.

INTRODUCTION

The seismic low-velocity zone (LVZ), beginning at a depth of ~80 km within Earth's mantle, has several important characteristics that may provide crucial clues to the fundamental physics of plate tectonics and mantle dynamics: (i) The seismic velocities decrease with depth within the LVZ, which is uncharacteristic of crystalline silicates as we know in the elastic regime. (ii) Globally, the LVZ exhibits maximum seismic anisotropy in the mantle, with the exception of the D″ layer. (iii) The LVZ is associated with a significant reduction in the seismic quality factor (Q). (iv) Electrical conductivity measurements report a marked increase in the LVZ. The origin of the LVZ has been under considerable debate in recent years. Although some authors argue that the LVZ may originate primarily from the decrease in elastic properties of solid peridotite under temperature conditions close to the solidus, without the involvement of partial melting (*1*–*4*) [hereafter referred to as the null hypothesis (*2*)], others mainly attribute its existence to the presence of small amounts of partial melt (*5*–*10*) (the partial melt hypothesis). Because the presence of melt significantly reduces the viscosity of rock aggregates (*11*) and modifies the compositions of the remaining crystals (*12*), the two hypotheses will lead to fundamentally different interpretations of the dynamics of plate tectonics (*13*).

Petrological analyses suggest that melts can remain gravitationally stable in the LVZ beneath the oceanic lithosphere (*7*, *12*, *14*) but only if the degree of partial melting does not exceed 0.1 to 0.2% in regions away from mid-ocean ridges. However, such low-degree partial melting, along with the experimentally observed wetting dihedral angles in basaltic melt (25° to 40°) (*15*), appears incompatible with the observed seismic velocity anomalies in the LVZ, which would require several percentages of partial melting. This has been used to support the null hypothesis (*1*–*4*). The arguments for this latter hypothesis assume that a melt phase is an unreactive component that can be accounted for by simple volume averaging, concluding that small amounts of melt do not have a large effect on seismic velocities. However, it is well known that melt microstructures (geometry of the melt pockets) and mobility play critical roles in modifying the physical and chemical properties of partially molten mineral assemblages (*11*, *16*, *17*). Both parameters are largely controlled by the composition of the mineral assemblage, the degree of partial melting, and the melt-solid dihedral angle (*18*). Earlier studies showed that, for a given composition, melts with complete wetting properties (that is, low dihedral angles) have significantly greater effects on the elastic wave velocities and seismic attenuation (*19*, *20*). These observations are used to support the partial melt hypothesis. The wetting behavior of the most geologically relevant basaltic melts is reported to produce a widespread network of melt upon partial melting, at pressures below 1 GPa (*15*). Because of experimental difficulties, the dynamic interaction between partial melts and the solid matrix under relevant mantle conditions (pressures at several gigapascals) has only begun to be explored (*21*).

The recent discovery of volcanism on ancient oceanic lithosphere (petit-spot volcanoes) (*22*–*25*) provides strong support for the partial melting hypothesis of the LVZ. The very young [generally <10 million years ago (Ma)] volcanic activities on old (ca. >100 Ma) oceanic plates indicate that fresh melts can segregate and erupt below the oceanic lithosphere, in regions far away from mid-ocean ridges. The depleted heavy rare-earth elements in petit-spot lavas indicate that the magma was derived from the garnet-bearing mantle, suggesting a source deeper than ~90 km (*26*), consistent with depths of the LVZ. Although seismic anisotropy of the LVZ appears to be consistent with both lattice-preferred orientation due to tectonic flow (*4*) in the null hypothesis and shape-preferred orientation of melt pockets (*10*) in the partial melt hypothesis, only the latter is capable of providing the needed source of fresh melt. Here, we report the results of a combined ultrasonic velocity and attenuation measurement at high pressure and high temperature to test the partial melt hypothesis in a dry olivine plus

[1]Laboratoire Magmas et Volcans, CNRS UMR 6524, Université Blaise Pascal, Institut de Recherche pour le Developpement, 63178 Clermont-Ferrand, France. [2]Center for Advanced Radiation Source, University of Chicago, Chicago, IL 60637, USA.
*Corresponding author. Email: julien.chantel@case.edu
†Present address: Department of Earth, Environmental and Planetary Sciences, Case Western Reserve University, Cleveland, OH 44106, USA.
‡Present address: Lawrence Livermore National Laboratory, Livermore, CA 94550, USA.

basalt system (see Materials and Methods for more details). Our data provide new experimental evidence under relevant pressure and temperature conditions of the LVZ, supporting the partial melt hypothesis.

RESULTS

Experimental procedure

Sound velocities of six different presynthesized polycrystalline samples were studied, including pure San Carlos (SC) olivine and SC olivine mixed with additional 0.1, 0.5, 1.0, 2.0, and 4.0 volume % of natural mid-ocean ridge basalt (MORB). The SC olivine sample is melt-free (Fig. 1A). In the sample with 0.1% MORB, melt pockets, observed after quenching from synthesis, are exclusively concentrated at triple junctions, and most grain boundaries are melt-free (Fig. 1B). For the sample with 0.5% MORB (Fig. 1C), the melt is distributed as a network on grain boundaries and occupies the triple junctions (*27*). Samples with higher MORB fractions exhibit more MORB across SC olivine grain boundaries (Fig. 1, D to F).

In situ travel time measurements of ultrasonic sound waves through the sintered aggregates were performed at 2.5 GPa up to 1623 K, which is higher than the melting temperature of the MORB component. High-pressure and high-temperature conditions were generated using the 1000-ton Kawai-type multianvil module (*28*) at the 13-ID-D beamline of GeoSoilEnviroCARS (GSECARS) at the Advanced Photon Source (APS). Energy-dispersive x-ray diffraction was used to determine sample pressure and to verify the sample state. Radiographic imaging was used to determine sample lengths in situ, yielding quantitative determination of sound velocities from the travel time measurements (see Materials and Methods for more details).

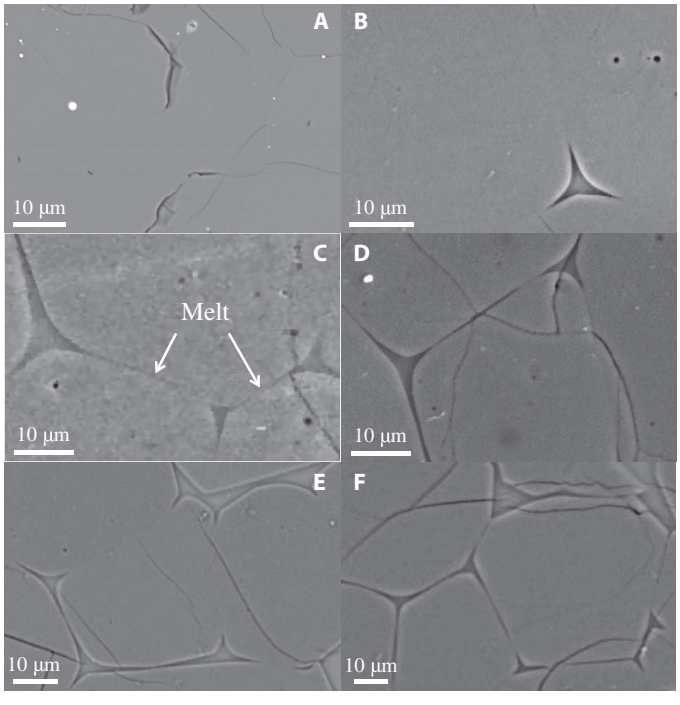

Fig. 1. Scanning electron microscope backscattered electron images showing melt distribution in samples. (**A**) Pure SC olivine. (**B**) 0.1% MORB. (**C**) 0.5% MORB. (**D**) 1% MORB. (**E**) 2% MORB. (**F**) 4% MORB. Black lines on the images are cracks developed during quenching and decompression. Note that the thickness of melt films at the grain boundaries increases with increasing melt fraction (φ) from 0.5 to 4.0% (C to F).

Effects of partial melt on V_P, V_S, and Q

We kept the temperature at 1623 K for up to 1 hour while continuously measuring V_P and V_S. In all experiments, V_P and V_S remained constant (Fig. 2 and table S1), within the uncertainties (±0.08 km·s^{-1} for V_P and ±0.05 km·s^{-1} for V_S), with no detectable effects or change in sample microstructure and melt texture during the experiments.

During the increase in temperature up to the melting point of the MORB (1573 K), all samples exhibit similar V_P and V_S within uncertainties (Fig. 2). Both V_P and V_S decrease slightly upon heating, as a consequence of the general decrease of bulk and shear moduli with temperature. These observations and the velocity data are consistent with previous velocity measurements on melt-free SC olivine aggregates (*29*). Once the melting of MORB is achieved, both V_P and V_S decrease sharply, with magnitudes of velocity decrease increasing with volume fraction of MORB in the sample (Fig. 3A). The magnitude of decrease is more pronounced in V_S than in V_P.

For all the compositions, amplitudes of both *P*- and *S*-wave echoes (Fig. 4) do not change significantly up to 1573 K. For SC olivine and 0.1% MORB samples, the amplitude of velocity echoes remains constant up to the highest investigated temperature of 1623 K. For samples with higher melt fractions (0.5, 1, 2, and 4% MORB), heating from 1573 to 1623 K results in a marked decrease in the amplitude of the *P*- and *S*-wave echoes by 8, 17, 17, and 17% for *P* waves and 22, 32, 47, and 50% for *S* waves, respectively. The variation is particularly pronounced for V_S, with a drop of 50% (compared to 17% for V_P) for the 4% MORB sample.

The decrease of amplitudes is related to the scattering of acoustic waves at the solid-liquid interfaces. *P*- and *S*-wave attenuations are assessed through the seismic quality factor (*Q*), which is proportional

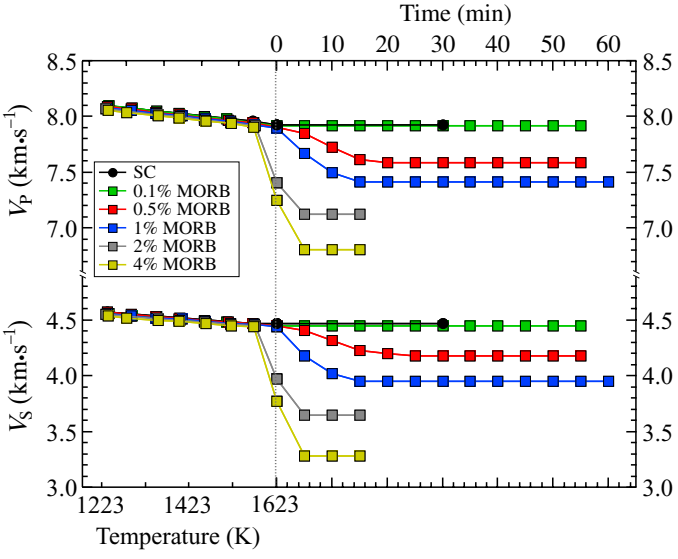

Fig. 2. *P*-wave (50 MHz) and *S*-wave (30 MHz) velocities as a function of increasing temperature, from 1273 to 1623 K (left part of the graph), and as a function of time at a constant temperature of 1623 K (right side of the graph), for the six compositions investigated in this study.

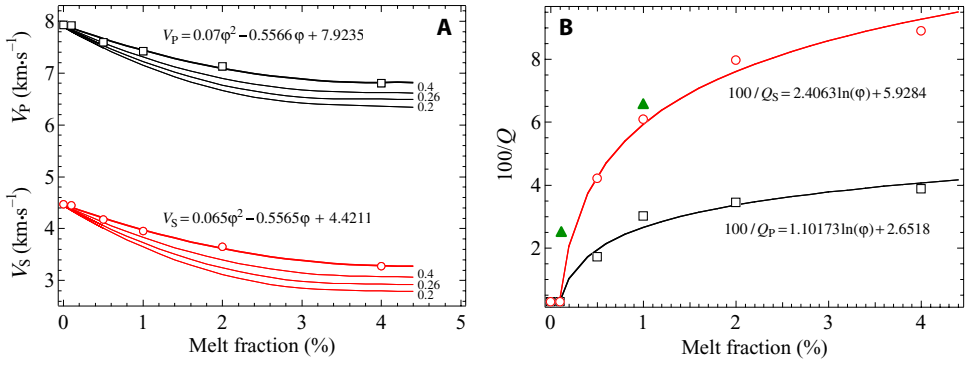

Fig. 3. Dependence of seismic properties on melt fraction. (**A** and **B**) Dependence of (A) V_P and V_S and (B) 100/Q on melt fraction. Open symbols are the experimental data and curves are the associated fits. In addition to our experimental results and their fits (thick curves), modeled velocities (thin curves) that include the anelastic effects expected for the seismic waves at high temperatures are reported in (A), using α values (from 0.2 to 0.4 shown in the graph) covering the entire range that was previously observed (*30*). In (B), the solid green triangles represent additional data from torsional experiments (*17*).

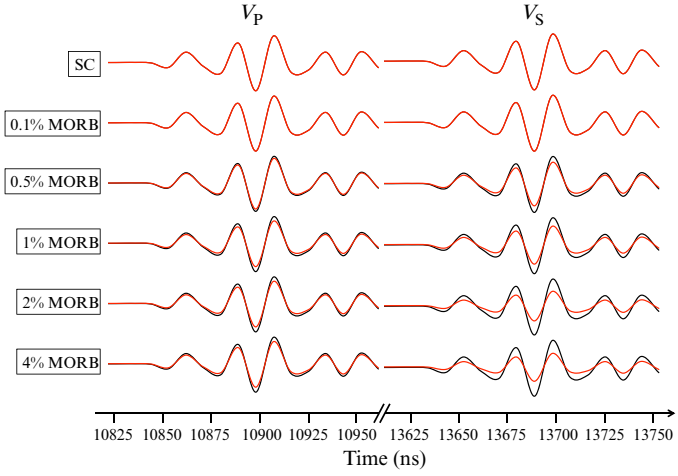

Fig. 4. *P*-wave (50 MHz) and *S*-wave (30 MHz) echoes recorded at 2.4 to 2.5 GPa for the six studied compositions. Black and red curves are signals at temperatures of 1573 and 1623 K, respectively. For SC olivine and 0.1% MORB, black and red curves completely overlap. Both *P*- and *S*-wave echoes (~100-ns time interval) were normalized with respect to the maximum amplitude of the echo from the buffer rod (BR) under the same pressure-temperature conditions.

to the attenuation factor (100/Q): $100/Q = 100/\left(2\pi\frac{\mathrm{Amp_{echo1}}}{\delta\mathrm{Amp}}\right)$, with δAmp = $\mathrm{Amp_{echo1}}$ − $\mathrm{Amp_{echo2}}$, where $\mathrm{Amp_{echo1}}$ and $\mathrm{Amp_{echo2}}$ are the respective amplitudes of the first and second echoes from the sample (see Materials and Methods for more details). Significant attenuation is detected for samples with MORB fraction φ ≥ 0.5%, and increasing MORB melt fraction raises the associated 100/Q_S values (Fig.3B). We fit the evolution of 100/Q_S as a function of φ using a logarithmic function, which reproduces the asymptotic trend for φ ≥ 2% very well. The value of 100/Q_S is 9 to 10 for V_S with 4 volume % of MORB.

Correction of V_P, V_S, and Q to seismic frequencies

To extrapolate our experimental measurements performed at megahertz frequencies to velocities at seismic frequencies, one must consider the effects of anelasticity on the velocities. Anharmonic effects, which affect thermal expansivity, generally involve no energy loss and are insensitive to the frequency of elastic waves. When the frequency (ω) of an elastic wave is comparable to, or shorter than, the characteristic frequency of relaxation, significant relaxation occurs, thereby affecting elastic wave velocities (*30*, *31*). Such anelastic effects on seismic velocities can be expressed using V_P, V_S, Q_P, and Q_S, from our experiments, with an empirical parameter α, which describes the frequency dependence of the quality factor ($Q \propto \omega^{\alpha}$) (*31*). Because of the low amount of melt expected for the mantle, we estimate seismic anelastic attenuation using the values of α reported for polycrystalline olivine (*30*).

It is usually assumed that for pure solids, dispersion effects are small up to megahertz frequencies (*18*), such that ultrasonic measurements yield relaxed velocities. On the other hand, many silicate melts have very high absorption in this frequency range, and signals are seriously attenuated over a distance as small as 2 mm (*32*, *33*). Nevertheless, a previous study (*32*) showed that the echo overlap technique, also used in our study, is suitable for high-Q melts, such as MORB. The minimum value of Q that was observed in pure silicate melts was 2.5, and the errors in the absorption calculations, even in this extreme case, were only 4% (*32*). However, in the referred study, multiple acoustic echoes were used to constrain Q (*32*). Here, we can observe only two subsequent echoes, which could significantly increase uncertainties. On the other hand, torsional experiments show that the superposition of melt-related dissipation results in nearly frequency-independent attenuation across the teleseismic frequency band (*17*). These torsional experimental data (*17*), performed on similar aggregates with various melt fractions, perfectly match the trend presented in Fig. 3B. Thus, it appears that assuming a much larger uncertainty of 10 to 20% in our measurements will not change the general trend in Fig. 3B: Most Q changes occur at very low melt fractions (~<2%); above 2%, there is only a modest further increase in 100/Q.

DISCUSSION

Properties of partially molten rocks strongly depend on the grain-scale melt distribution. A major controlling parameter is the equilibrium dihedral angle (θ), which changes with composition of the melt (*26*). Here, the samples were treated under identical experimental conditions [2.5 (±1) GPa and 1623 K], with MORB content varying slightly in the SC olivine matrix; thus, it can be safely assumed that θ

remains constant for all experiments. Our acoustic velocity and attenuation measurements show a gradual change in the melt distribution as a function of melt fraction (Fig. 3, A and B). When melt fraction is lower than 0.001 (0.1% MORB), grain boundaries are melt-free (Fig. 1B); hence, the effect of melt on the sound velocities is negligible (fig. S2). When melt fraction is higher ($\varphi > 0.1\%$), wave propagation is affected by melt-wetted boundaries of olivine grains, resulting in lower velocities. As previously reported in the simple binary system composed of NaCl + H_2O (*20*), compressional and shear velocities exhibited a drop of 9.5 and 13.5%, respectively, compared to the solid assemblage, when 3.3% of melt (H_2O in that study) was present. Meanwhile, attenuation increased by 37 and 48% for $100/Q_P$ and $100/Q_S$, respectively. Similar behavior is observed in our samples. If we interpolate the results from the present study to 3.3 volume % of MORB, we estimate velocity drops of 13.7% for ΔV_P and 24.9% for ΔV_S, and the attenuation, $100/Q_P$ and $100/Q_S$, increases by 12.3 and 29.3%, respectively, compared to the solid SC olivine sample. These similarities between the two very different systems confirm that a small amount of melt can significantly affect the elastic and anelastic properties of partially molten materials.

In the LVZ, velocity reductions are approximately 2% for V_P and from 5 to 8% for V_S, with attenuation increasing by a factor of 3 or more (*34*–*37*). The depth of the upper LVZ boundary, approximately the lithosphere-asthenosphere boundary, has recently been refined by compiling teleseismic data at two observatories to be ~80 km (*10*). Waveform modeling indicates an abrupt reduction of the shear wave velocity by ~7 to 8% (*10*). To enable a quantitative comparison between our experimental measurements and the seismological features, some major factors must be taken into consideration: (i) At the high frequencies used in our experiments, the material remains unrelaxed and therefore appears stiffer, giving higher velocity values. In contrast, seismic frequencies are much lower, allowing the material to relax, hence yielding lower velocities. As discussed above, however, the difference between experimental and mantle velocities can be modeled using the anelastic attenuation factor (α). (ii) In our experiments, the solid phase is olivine, as opposed to a peridotitic mixture of minerals in the upper mantle. Thus, V_P and V_S corresponding to 0% melt are intrinsically different, making a direct comparison difficult between experimental and seismic V_P and V_S (see fig. S3). Still, relative changes in seismic properties due to the presence of melt should be comparable in the two systems (olivine plus MORB in the laboratory versus peridotitic plus partial melt in the LVZ). For a range of values of α, the seismic velocities are well matched by melt fractions of 0.1 to 0.3% and 0.2 to 0.4% for V_P and V_S, respectively, based on our experimental data (fig. S3).

Because *P*- and *S*-wave velocities have different sensitivities to partial melt, temperature, and composition, a combination of V_P and V_S provides more insight into mantle physical state than either V_P or V_S alone. In particular, V_S is more sensitive to the presence of melt than V_P (while being similarly sensitive to composition and temperature); hence, the V_P/V_S ratio can provide additional constraints to probe the mantle state and distinguish regions of partial melt. Although major minerals of the LVZ (olivine, garnets, and pyroxenes) show relatively low V_P/V_S ratios [values generally ranging from 1.7 to 1.8 (*38*)], melt fractions between 0 and 0.5% are consistent with high V_P/V_S ratios of global seismic models of the LVZ [PREM (*39*), IASP91 (*40*), and Ak135 (*41*)], for a broad range of α values (Fig. 5A). Our predicted V_P/V_S ratio increases rapidly with increasing melt fraction (from 1.8 to 2.2 for φ from 0.1 to 4%; see Fig. 5A). Most seismic models give V_P/V_S ratios from 1.8 to 1.9 for the LVZ which is consistent with melt

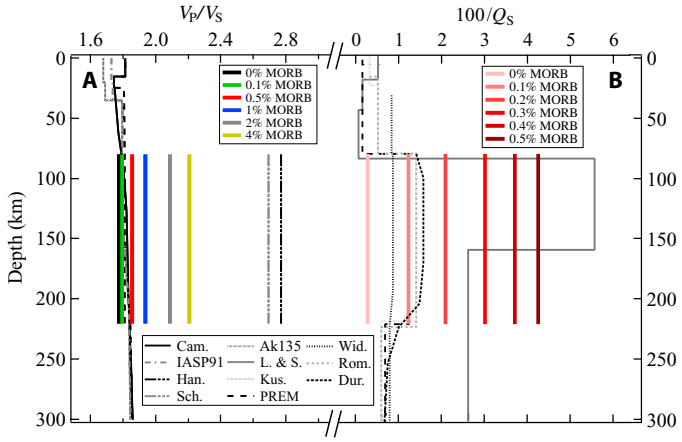

Fig. 5. Empirical profiles, calculated for various melt fractions, compared to seismic profiles. (**A**) V_P/V_S ratio as a function of melt compared to global earth models (*39*–*41*, *68*) and regional seismic profiles (*42*, *43*), for an anelasticity attenuation factor $\alpha = 0.26$. (**B**) Reported seismic profiles of attenuation compared with empirical profiles calculated for melt fractions ranging from 0 to 0.5%, based on our experimental results and for an anelasticity attenuation factor $\alpha = 0.26$. Global seismic models (*35*–*37*, *39*–*41*) and regional seismic profiles (*69*, *70*). The nonlinear evolution of $100/Q_S$ as a function of φ is due to the logarithmic fitting used (Fig. 3B).

fractions of 0.1 to 0.5%. To reach values as high as 2.5 to 2.77, as reported in some local seismic studies (*42*, *43*), unrealistic melt fractions of 10 to 20% are required. An alternative explanation of these unusually high V_P/V_S regions would be the enrichment of volatiles (such as CO_2 and/or H_2O) that would change the wetting properties of the melt.

Figure 5B shows that most seismic models give $100/Q_S$ values on the order of 1, which can also be explained well by partial melt with a melt fraction between 0.1 and 0.2%. Some controversial local models, such as the very high values of $100/Q_S$ of 5.5 (*34*), may require greater volatile contents in the LVZ.

Considering electrical conductivity data for the LVZ, experimental results (*44*) show that ~1% basalt melt in olivine is required to increase the electrical conductivity by one order of magnitude (from ~$10^{-2.2}$ to ~0.1 S/m), in dry systems. Electrical conductivity has not been carefully considered in previous analyses, especially in papers supporting the "null hypothesis" (*2*, *4*). Those studies (*2*, *4*) critique the partial melt hypothesis, but they neglected electrical conductivity in their arguments for the null hypothesis: the null hypothesis cannot explain the observed electrical conductivity anomaly. However, small amounts of volatiles, such as CO_2 or H_2O, can significantly increase electrical conductivity (*44*–*47*). A previous study (*47*) shows that a combination of 200–parts per million (ppm) H_2O and 200-ppm CO_2 (distributed in the melt and very similar to the 165-ppm CO_2 in our study) can produce electrical conductivity anomaly by a factor of 10 at 1523 to 1623 K, with 0.1 to 0.2% partial melt. The range of partial melt inferred from the present study is also consistent with those of conductivity models. A combination of our study plus electrical conductivity investigation (*47*) provides extremely strong support for the partial melt hypothesis.

In summary, experimentally determined velocities, V_P/V_S ratio, and attenuation $100/Q_S$ of rock assemblies consisting of solid SC olivine and molten basalt can all be compared directly with seismological observations of the LVZ, after correcting anelastic effects. The inferred amounts of partial melt, at 0.1 to 0.3% levels, are also consistent with

petrological observations (*12*) as well as current electrical conductivity models (*47*). Thus, we conclude that low–melt-fraction partial melt remains a viable physical origin for the LVZ.

The LVZ, if indeed originated from partial melt, will be the layer with the lowest viscosity values of the mantle (*48*). Perhaps not coincidentally, Sakamaki *et al.* (*49*) show that for basaltic melts, viscosity decreases with depth and melt mobility peaks in the asthenosphere. The relative motion of the rigid plates over the rheologically weak asthenosphere imposes shear deformation in the LVZ, forming laminated lithologies and aligned melt accumulations [LLAMAs (*50*, *51*)], which further weakens the LVZ, thereby decoupling the lithosphere from the underlying mantle (*52*, *53*). Shearing in the melt-rich layer causes melt segregation and stress concentrations that facilitate continuous reconstitution of the LVZ and the formation of dikes, which, in turn, are responsible for intraplate volcanism (*54*, *55*).

Geodynamic models suggest that the coupling strength between tectonic plates and the underlying mantle is inversely proportional to the viscosity in the LVZ (*50*), and plate boundaries and plate tectonics are controlled by lateral heterogeneities in the lithosphere-LVZ decoupling (*54*). Melt migration is an effective way of generating lateral heterogeneities in the lithosphere-LVZ coupling/decoupling cycle. After losing the melt in the LLAMAs through volcanic activities, the LVZ will become more viscous, and plate motion will slow down, or even stop, until laterally passive mantle upwelling refuels melt in the LVZ to introduce new LLAMAs again (*54*). This may be a controlling factor for the Wilson cycle, which addresses the evolution with the geological time of the plate motions, from opening at mid-oceanic ridges to contraction at the subduction zones.

MATERIALS AND METHODS

Starting material

We conducted velocity measurements on six different polycrystalline samples, including pure SC olivine (<100-ppm H_2O) and SC olivine with additional 0.1, 0.5, 1.0, 2.0, and 4.0 volume % of natural MORB. Basalt was collected at a 2800-m depth during the Searise-1 research cruise and contains 2700 ppm of H_2O and 165 ppm of CO_2 (*56*). The melt fraction of the sample was controlled by the amount of MORB mixed with SC olivine. The MORB glass and the inclusion-free, hand-picked SC olivine crystals were crushed and reduced to fine-grain powders (<63 μm), and these powders were then mixed with predetermined weight proportions to obtain a solid-plus-melt system with a controlled melt fraction. The powder mixtures were ground with ethanol in an agate mortar for 1 to 2 hours and dried, ensuring the homogeneity of the starting mixture.

Samples were hot-pressed into a cylindrical shape at 3 GPa and 1273 K for 2 hours, using a 1500-ton split-sphere multianvil apparatus at the Laboratoire Magmas et Volcans. The top and bottom surfaces of each sample were polished and analyzed using a scanning electron microscope (SEM) to determine purity and grain size, which was found to be <50 μm. We also measured the density of the samples using the Archimedes immersion method and confirmed that the sintered samples had almost zero porosity.

Synthetic samples for ultrasonic wave propagation velocity measurement must satisfy the following conditions to produce strong acoustic reflections with high signal-to-noise ratio during ultrasonic wave propagation measurements. According to Mason and McSkimin (*57*), the attenuation of a propagated wave depends on grain size a and wavelength λ; the larger the grain size, the higher the attenuation. In addition, if the sample has large grain sizes, crystals in the sample will tend to form a preferred orientation, making the sample anisotropic. Liebermann *et al.* (*58*) showed that the ratio λ/a must exceed 2. In our study, 2.7 (20 MHz) < λ/a < 8 (60 MHz). These λ/a values are the lower bound, as SEM analyses showed that the actual average grain size is <50 μm, leading to higher λ/a ratio values. According to Birch (*59*), the length/diameter aspect ratio (l/d) of the specimen should not exceed 0.5 for reliable P-wave measurements. Larger values of l/d will seriously affect recorded acoustic signals due to boundary reflections. Here, $l \approx 0.8$ mm and $d \approx 2$ mm; hence, $l/d \approx 0.4$. Finally, previous studies (*60*, *61*) show that, depending on the relationship between the sample diameter and the wavelength of the elastic waves propagating through the sample, the measured P-wave velocity can be that of longitudinal waves in an infinite medium V_{PM}, in a plate V_{PPL}, or in a thin rod V_{PR}. To warrant that the measured velocity in our sound velocity propagation studies is indeed V_{PM}, the ratio d/λ must not fall below 2.4. For our samples, 5 (20 MHz) < d/λ< 15 (60 MHz).

Effects of potential volatiles partitioning from the melt into the olivine aggregate, which tend to affect the bulk velocities and Q values of the sample, should be small. Considering an exchange of water between the basaltic melt and olivine, occurring after melting in the sample containing the maximum MORB content (4 volume %), using a partitioning coefficient $D_{H2O}^{Ol/melt} = 0.002$ (*62*), the water content in the olivine aggregate will increase by less than 0.3 ppm. This is negligible considering the initial water content (<100 ppm) in the olivine crystals. A previous study (*63*) showed that the H_2O contents must be >10 ppm to have an observable change in velocities and Q values. The fact that no velocity change was observed [after being kept at high pressure and high temperature for 1 hour (before melting)] also indicates that there was no volatile exchange between olivine and MORB, at least in the solid state.

Equilibrium melt textures in olivine-basalt systems have been investigated in a number of previous studies (*27*, *46*, *64*). In the equilibrium state, dominant melt geometries are grain boundary melt films and triple-junction networks (*27*) or ellipsoidal discs (*64*). Here, the melt composition remained constant at fixed pressure and temperature (2.5 GPa and 1623 K). Also, the relatively constant velocity upon the melting of MORB components suggests that melt fraction did not increase with time because an increase of melt fraction would result in a decrease of velocity.

Synchrotron experiments

In situ travel time measurements of ultrasonic sound waves through the sintered, polycrystalline aggregates were performed at 2.5 GPa up to 1623 K. High-pressure and high-temperature conditions were generated using the 1000-ton Kawai-type T-25 multianvil module (*28*) at the 13-ID-D beamline of GSECARS at the APS. Energy-dispersive x-ray diffraction was used to determine the sample pressure and verify the sample state. In all of the experiments, we clearly observed the diffraction peaks typical of our sample and not a broad band of diffuse scattering as described previously elsewhere (*65*). This is due to the degree of partial melting that remained low at all experimental conditions performed in this study. Simultaneously, we acquired radiographic images for the determination of the sample lengths, yielding accurate quantitative determination of sound velocities from the travel time measurements.

In situ multianvil assembly

An injection-molded octahedral MgO-$MgAl_2O_4$ pressure medium with a 14-mm edge length (*66*) was used in each experiment (fig. S1). Our assemblage includes a dense Al_2O_3 BR placed between the WC anvil and the sample, primarily to enhance the propagation of elastic waves and to provide sufficient impedance contrast to reflect ultrasonic waves at the BR-sample interface. Both ends of the anvil, BR, and samples were carefully polished using 0.25-μm diamond pastes to enhance mechanical contacts. The sample was placed in an MgO sleeve capsule and backed by an MgO plus Pt mixture [backing material (BM)], which was used as pressure markers. Pressure was determined from the MgO and Pt mixture (MgO/Pt = 20:1 by volume), using the equations of state (*67*). Samples were annealed at 1373 K for 30 min to 1 hour before the sound wave velocity measurements to ensure full relaxation of the deviatoric stresses. The sample temperature was measured using a W_5Re-$W_{26}Re$ thermocouple. The uncertainties in pressure and temperature are about 0.5 GPa and 50 K, respectively.

Ultrasonic measurements

The experimental setup used for in situ ultrasonic measurements on partially molten samples is the same as previously described (*65*). The 10° *Y*-cut $LiNbO_3$ piezoelectric transducer was attached to the back of the WC anvil using high-temperature epoxy resin. The resonant frequency of the transducer is 50 MHz for compressional waves (*P* waves) and 30 MHz for shear waves (*S* waves). Electrical signals of sine waves of 20 to 60 MHz (three cycles) with a $V_{peak\text{-}to\text{-}peak}$ of 1 V were generated using an arbitrary waveform generator and were converted to *P* and *S* waves by the transducer. Elastic waves propagated through the anvil, BR, and samples and were reflected back at the anvil-BR, BR-sample, and sample-BM interfaces. The reflected elastic waves were converted back to electrical signals by the transducer and amplified by a 40-dB preamplifier with a bandwidth of 0.2 to 40 MHz before being captured by a digital oscilloscope at a sampling rate of 5×10^9 samples per second. The high amplitude of the input signal used a directional bridge to avoid damaging the oscilloscope. Uncertainties in sound velocities are estimated to be 2%, which come mainly from the uncertainties in sample length measurements. We applied various frequencies from 20 to 60 MHz to examine the frequency dependence of velocities.

To determine *Q*, we first normalized both *P*- and *S*-wave echoes with respect to the maximum amplitude of the echo from the BR under the same pressure-temperature conditions. Then, we used the amplitude of the signals from the sample, corresponding to the first and second echo generated at the sample-BM interface, Amp_{echo1} and Amp_{echo2}, respectively (fig. S4).

SUPPLEMENTARY MATERIALS

Supplementary material for this article is available at http://advances.sciencemag.org/cgi/content/full/2/5/e1600246/DC1

fig. S1. Schematic drawing of the cell assembly used in the multianvil experiments.

fig. S2. Reduction of *S*- and *P*-wave velocities as a function of melt fraction.

fig. S3. Seismic profiles of V_P, V_S, and $100/Q_S$ compared with empirical profiles, calculated for various melt fractions, based on the experimental results from this study and for an anelasticity attenuation factor $\alpha = 0.26$ (*30*).

fig. S4. Ultrasonic signal recorded at 30 MHz.

table S1. Experimental conditions and the results.

Reference (*71*)

REFERENCES AND NOTES

1. S.-i. Karato, H. Jung, Water, partial melting and the origin of the seismic low velocity and high attenuation zone in the upper mantle. *Earth Planet. Sci. Lett.* **157**, 193–207 (1998).
2. L. Stixrude, C. Lithgow-Bertelloni, Mineralogy and elasticity of the oceanic upper mantle: Origin of the low-velocity zone. *J. Geophys. Res.* **110**, B03204 (2005).
3. K. Priestley, D. McKenzie, The relationship between shear wave velocity, temperature, attenuation and viscosity in the shallow part of the mantle. *Earth Planet. Sci. Lett.* **381**, 78–91 (2013).
4. S.-i. Karato, Does partial melting explain geophysical anomalies? *Phys. Earth Planet. Inter.* **228**, 300–306 (2014).
5. I. B. Lambert, P. J. Wyllie, Stability of hornblende and a model for the low velocity zone. *Nature* **219**, 1240–1241 (1968).
6. D. L. Anderson, H. Spetzler, Partial melting and the low-velocity zone. *Phys. Earth Planet. Inter.* **4**, 62–64 (1970).
7. D. C. Presnall, G. H. Gudfinnsson, M. J. Walter, Generation of mid-ocean ridge basalts at pressures from 1 to 7 GPa. *Geochim. Cosmochim. Acta* **66**, 2073–2090 (2002).
8. K. Mierdel, H. Keppler, J. R. Smyth, F. Langenhorst, Water solubility in aluminous orthopyroxene and the origin of Earth's asthenosphere. *Science* **315**, 364–368 (2007).
9. Y. Tan, D. V. Helmberger, Trans-Pacific upper mantle shear velocity structure. *J. Geophys. Res.* **112**, B08301 (2007).
10. H. Kawakatsu, P. Kumar, Y. Takei, M. Shinohara, T. Kanazawa, E. Araki, K. Suyehiro, Seismic evidence for sharp lithosphere-asthenosphere boundaries of oceanic plates. *Science* **324**, 499–502 (2009).
11. T. T. Gribb, R. F. Cooper, Low-frequency shear attenuation in polycrystalline olivine: Grain boundary diffusion and the physical significance of the Andrade model for viscoelastic rheology. *J. Geophys. Res.* **103**, 27267–27279 (1998).
12. T. Plank, C. H. Langmuir, Effects of melting regime on the composition of the oceanic crust. *J. Geophys. Res.* **97**, 19749–19770 (1992).
13. M. A. Richards, W.-S. Yang, J. R. Baumgardner, H.-P. Bunge, Role of a low-viscosity zone in stabilizing plate tectonics: Implications for comparative terrestrial planetology. *Geochem. Geophys. Geosyst.* **2**, 1026 (2001).
14. M. M. Hirschmann, Partial melt in the oceanic low velocity zone. *Phys. Earth Planet. Inter.* **179**, 60–71 (2010).
15. D. L. Kohlstedt, Structure, rheology and permeability of partially molten rocks at low melt fractions, in *Mantel Flow and Melt Generations at Mid-Ocean Ridges*, J. P. Morgan, D. K. Blackman, J. M. Sinton, Eds. (American Geophysical Union, Washington, DC, 1992), pp. 103–122.
16. W. C. Hammond, E. D. Humphreys, Upper mantle seismic wave velocity: Effects of realistic partial melt geometries. *J. Geophys. Res.* **105**, 10975–10986 (2000).
17. U. H. Faul, J. D. F. Gerald, I. Jackson, Shear wave attenuation and dispersion in melt-bearing olivine polycrystals: 2. Microstructural interpretation and seismological implications. *J. Geophys. Res.* **109**, B06202 (2004).
18. R. L. Stocker, R. B. Gordon, Velocity and internal friction in partial melts. *J. Geophys. Res.* **80**, 4828–4836 (1975).
19. H. Mizutani, H. Kanamori, Variation of elastic wave velocity and attenuative property near the melting temperature. *J. Phys. Earth* **12**, 43–49 (1964).
20. H. Spetzler, D. L. Anderson, The effect of temperature and partial melting on velocity and attenuation in a simple binary system. *J. Geophys. Res.* **73**, 6051–6060 (1968).
21. L. Li, D. J. Weidner, Effect of dynamic melting on acoustic velocities in a partially molten peridotite. *Phys. Earth Planet. Inter.* **222**, 1–7 (2013).
22. N. Hirano, A. A. P. Koppers, A. Takahashi, T. Fujiwara, M. Nakanishi, Seamounts, knolls and petit-spot monogenetic volcanoes on the subducting Pacific Plate. *Basin Res.* **20**, 543–553 (2008).
23. N. Hirano, Petit-spot volcanism: A new type of volcanic zone discovered near a trench. *Geochem. J.* **45**, 157–167 (2011).
24. N. Hirano, S. Machida, N. Abe, T. Morishita, A. Tamura, S. Arai, Petit-spot lava fields off the central Chile trench induced by plate flexure. *Geochem. J.* **47**, 249–257 (2013).
25. J. Yamamoto, J. Korenaga, N. Hirano, H. Kagi, Melt-rich lithosphere-asthenosphere boundary inferred from petit-spot volcanoes. *Geology* **42**, 967–970 (2014).
26. J. G. Arth, Behaviour of trace elements during magmatic processes: A summary of theoretical models and their applications. *J. Res. U.S. Geol. Surv.* **4**, 41–47 (1976).
27. D. A. Wark, C. A. Williams, E. B. Watson, J. D. Price, Reassessment of pore shapes in microstructurally equilibrated rocks, with implications for permeability of the upper mantle. *J. Geophys. Res.* **108**, 2050 (2003).
28. Y. Wang, M. Rivers, S. Sutton, N. Nishiyama, T. Uchida, T. Sanehira, The large-volume high-pressure facility at GSECARS: A "Swiss-army-knife" approach to synchrotron-based experimental studies. *Phys. Earth Planet. Inter.* **174**, 270–281 (2009).
29. W. Liu, J. Kung, B. Li, Elasticity of San Carlos olivine to 8 GPa and 1073 K. *Geophys. Res. Lett.* **32**, L16301 (2005).
30. I. Jackson, J. D. Fitz Gerald, U. H. Faul, B. H. Tan, Grain-size-sensitive seismic wave attenuation in polycrystalline olivine. *J. Geophys. Res.* **107**, 2360 (2002).

31. S.-i. Karato, Importance of anelasticity in the interpretation of seismic tomography. *Geophys. Res. Lett.* **20**, 1623–1626 (1993).
32. M. L. Rivers, I. S. E. Carmichael, Ultrasonic studies of silicate melts. *J. Geophys. Res.* **92**, 9247–9270 (1987).
33. V. C. Kress, Q. Williams, I. S. E. Carmichael, Ultrasonic investigation of melts in the system Na_2O-Al_2O_3-SiO_2. *Geochim. Cosmochim. Acta* **52**, 283–293 (1988).
34. D. L. Anderson, C. Sammis, Partial melting in the upper mantle. *Phys. Earth Planet. Inter.* **3**, 41–50 (1970).
35. J. J. Durek, G. Ekström, A radial model of anelasticity consistent with long-period surface-wave attenuation. *B. Seismol. Soc. Am.* **86**, 144–158 (1996).
36. R. Widmer, G. Masters, F. Gilbert, Spherically symmetric attenuation within the Earth from normal mode data. *Geophys. J. Int.* **104**, 541–553 (1991).
37. B. Romanowicz, A global tomographic model of shear attenuation in the upper mantle. *J. Geophys. Res.* **100**, 12375–12394 (1995).
38. Y. Takei, Effect of pore geometry on V_P/V_S: From equilibrium geometry to crack. *J. Geophys. Res.* **107**, ECV 6-1–ECV 6-12 (2002).
39. A. M. Dziewonski, D. L. Anderson, Preliminary reference Earth model. *Phys. Earth Planet. Inter.* **25**, 297–356 (1981).
40. B. L. N. Kennett, E. R. Engdahl, Traveltimes for global earthquake location and phase identification. *Geophys. J. Int.* **105**, 429–465 (1991).
41. B. L. N. Kennett, E. R. Engdahl, R. Buland, Constraints on seismic velocities in the Earth from traveltimes. *Geophys. J. Int.* **122**, 108–124 (1995).
42. A. J. Schaeffer, M. G. Bostock, A low-velocity zone atop the transition zone in Northwestern Canada. *J. Geophys. Res.* **115**, B06302 (2010).
43. R. T. J. Hansen, M. G. Bostock, N. I. Christensen, Nature of the low velocity zone in Cascadia from receiver function waveform inversion. *Earth Planet. Sci. Lett.* **337–338**, 25–38 (2012).
44. H. Ni, H. Keppler, H. Behrens, Electrical conductivity of hydrous basaltic melts: Implications for partial melting in the upper mantle. *Contrib. Mineral. Petrol.* **162**, 637–650 (2011).
45. K. J. Miller, L. G. J. Montési, W.-. Zhu, Estimates of olivine–basaltic melt electrical conductivity using a digital rock physics approach. *Earth Planet. Sci. Lett.* **432**, 332–341 (2015).
46. T. Yoshino, M. Laumonier, E. McIsaac, T. Katsura, Electrical conductivity of basaltic and carbonatite melt-bearing peridotites at high pressures: Implications for melt distribution and melt fraction in the upper mantle. *Earth Planet. Sci. Lett.* **295**, 593–602 (2010).
47. D. Sifré, E. Gardés, M. Massuyeau, L. Hashim, S. Hier-Majumder, F. Gaillard, Electrical conductivity during incipient melting in the oceanic low-velocity zone. *Nature* **509**, 81–85 (2014).
48. Z.-M. Jin, H. W. Green, Y. Zhou, Melt topology in partially molten mantle peridotite during ductile deformation. *Nature* **372**, 164–167 (1994).
49. T. Sakamaki, A. Suzuki, E. Ohtani, H. Terasaki, S. Urakawa, Y. Katayama, K.-. Funakoshi, Y. Wang, J. W. Hernlund, M. D. Ballmer, Ponded melt at the boundary between the lithosphere and asthenosphere. *Nat. Geosci.* **6**, 1041–1044 (2013).
50. C. Doglioni, A. Ismail-Zadeh, G. Panza, F. Riguzzi, Lithosphere–asthenosphere viscosity contrast and decoupling. *Phys. Earth Planet. Inter.* **189**, 1–8 (2011).
51. S. French, V. Lekic, B. Romanowicz, Waveform tomography reveals channeled flow at the base of the oceanic asthenosphere. *Science* **342**, 227–230 (2013).
52. C. H. Craig, D. McKenzie, The existence of a thin low-viscosity layer beneath the lithosphere. *Earth Planet. Sci. Lett.* **78**, 420–426 (1986).
53. C. P. Conrad, B. Wu, E. I. Smith, T. A. Bianco, A. Tibbetts, Shear-driven upwelling induced by lateral viscosity variations and asthenospheric shear: A mechanism for intraplate volcanism. *Phys. Earth Planet. Inter.* **178**, 162–175 (2010).
54. C. Doglioni, D. L. Anderson, Top-driven asymmetric mantle convection, in *The Interdisciplinary Earth: A Volume in Honor of Don L. Anderson*, G. R. Fougler, M. Lustrino, S. D. King, Eds. (Geological Society of America, Boulder, CO, 2015), pp. 51–63.
55. N. Hirano, E. Takahashi, J. Yamamoto, N. Abe, S. P. Ingle, I. Kaneoka, T. Hirata, J.-I. Kimura, T. Ishii, Y. Ogawa, S. Machida, K. Suyehiro, Volcanism in response to plate flexure. *Science* **313**, 1426–1428 (2006).
56. D. Andrault, G. Pesce, M. A. Bouhifd, N. Bolfan-Casanova, J.-M. Hénot, M. Mezouar, Melting of subducted basalt at the core-mantle boundary. *Science* **344**, 892–895 (2014).
57. W. P. Mason, H. J. McSkimin, Attenuation and scattering of high frequency sound waves in metals and glasses. *J. Acoust. Soc. Am.* **19**, 464–473 (1947).
58. R. C. Liebermann, A. E. Ringwood, D. J. Mayson, A. Major, Hot-pressing of polycrystalline aggregates at very high pressure for ultrasonic measurements, Proceedings of the 4th International Conference on High Pressure, Kyoto, 25 to 29 November 1974, pp. 495–502.
59. F. Birch, The velocity of compressional waves in rocks to 10 kilobars: 1. *J. Geophys. Res.* **65**, 1083–1102 (1960).
60. O. I. Silaeva, O. G. Shamina, The distribution of elastic pulses in cylindrical specimens. *Bull. Acad. Sci. USSR Geophys. Ser.*, 17–24 (1958).
61. L. Y. Tu, J. N. Brennan, J. A. Sauer, Dispersion of ultrasonic pulse velocity in cylindrical rods. *J. Acoust. Soc. Am.* **27**, 550–555 (1955).
62. D. Novella, D. J. Frost, E. H. Hauri, H. Bureau, C. Raepsaet, M. Roberge, The distribution of H_2O between silicate melt and nominally anhydrous peridotite and the onset of hydrous melting in the deep upper mantle. *Earth Planet. Sci. Lett.* **400**, 1–13 (2014).
63. Y. Aizawa, A. Barnhoorn, U. H. Faul, J. D. F. Gerald, I. Jackson, The influence of water on seismic wave attenuation in dunite: An exploratory study. *J. Petrol.* **49**, 841–855 (2008).
64. U. H. Faul, D. R. Toomey, H. S. Waff, Intergranular basaltic melt is distributed in thin, elongated inclusions. *Geophys. Res. Lett.* **21**, 29–32 (1994).
65. Z. Jing, Y. Wang, Y. Kono, T. Yu, T. Sakamaki, C. Park, M. L. Rivers, S. R. Sutton, G. Shen, Sound velocity of Fe–S liquids at high pressure: Implications for the Moon's molten outer core. *Earth Planet. Sci. Lett.* **396**, 78–87 (2014).
66. K. D. Leinenweber, J. A. Tyburczy, T. G. Sharp, E. Soignard, T. Diedrich, W. B. Petuskey, Y. Wang, J. L. Mosenfelder, Cell assemblies for reproducible multi-anvil experiments (the COMPRES assemblies). *Am. Mineral.* **97**, 353–368 (2012).
67. Y. Fei, J. Li, K. Hirose, W. Minarik, J. Van Orman, C. Sanloup, W. van Westrenen, T. Komabayashi, K.-. Funakoshi, A critical evaluation of pressure scales at high temperatures by in situ X-ray diffraction measurements. *Phys. Earth Planet. Inter.* **143–144**, 515–526 (2004).
68. F. Cammarano, A. Deuss, S. Goes, D. Giardini, One-dimensional physical reference models for the upper mantle and transition zone: Combining seismic and mineral physics constraints. *J. Geophys. Res.* **110**, B01306 (2005).
69. W. B. Lee, S. C. Solomon, Simultaneous inversion of surface wave phase velocity and attenuation: Love waves in western North America. *J. Geophys. Res.* **83**, 3389–3400 (1978).
70. B. Kustowski, G. Ekström, A. M. Dziewoński, Anisotropic shear-wave velocity structure of the Earth's mantle: A global model. *J. Geophys. Res.* **113**, B06306 (2008).
71. Q. Williams, E. J. Garnero, Seismic evidence for partial melt at the base of Earth's mantle. *Science* **273**, 1528–1530 (1996).

Acknowledgments: We thank J.-M. Henot for his assistance with the SEM analyses. **Funding:** Parts of this work were performed at GSECARS (Sector 13), APS, Argonne National Laboratory. GSECARS was supported by the NSF–Earth Sciences (EAR-1128799) and the Department of Energy–Geosciences (DE-FG02-94ER14466). Use of the APS was supported by the U.S. Department of Energy, Office of Science, Office of Basic Energy Sciences, under contract DE-AC02-06CH11357. G.M. acknowledges funding from the French PNP program (Institut National des Sciences de l'Univers–CNRS) and the Actions initiatives OPGC 2014. Y.W. acknowledges financial support from the NSF under EAR-1214376. This research was financed by the French Government Laboratory of Excellence initiative no. ANR-10-LABX-0006, the Région Auvergne, and the European Regional Development Fund. This is Laboratory of Excellence ClerVolc contribution number 174. **Author contributions:** J.C., G.M., and D.A. organized the research project. J.C., G.M., and D.N collected and analyzed the data. Y.W. and T.Y. provided technical support at GSECARS (Sector 13), APS, Argonne National Laboratory. J.C. wrote the paper, and all authors discussed the results and commented on the manuscript. **Competing interests:** The authors declare that they have no competing interests. **Data and materials availability:** All data needed to evaluate the conclusions in the paper are present in the paper and/or the Supplementary Materials. Additional data related to this paper may be requested from the authors.

Submitted 5 February 2016
Accepted 27 April 2016
Published 20 May 2016
10.1126/sciadv.1600246

Citation: J. Chantel, G. Manthilake, D. Andrault, D. Novella, T. Yu, Y. Wang, Experimental evidence supports mantle partial melting in the asthenosphere. *Sci. Adv.* **2**, e1600246 (2016).